Interactions, Morphology and Thermal Stability of Graphene-Oxide Reinforced Polymer Aerogel Derived from Star-Like Telechelic Aldehyde-Terminal Benzoxazine Resin

Article *in* RSC Advances · October 2015

DOI: 10.1039/C5RA16188F

CITATIONS
25

READS
1,898

5 authors, including:

Almahdi A Alhwaige
Elmergib University
19 PUBLICATIONS **471** CITATIONS
SEE PROFILE

Saeed M Alhassan
Khalifa University
230 PUBLICATIONS **3,930** CITATIONS
SEE PROFILE

Marios S. Katsiotis
TITAN Cement S.A.
71 PUBLICATIONS **753** CITATIONS
SEE PROFILE

Hatsuo Ishida
Case Western Reserve University
528 PUBLICATIONS **26,507** CITATIONS
SEE PROFILE

RSC Advances

PAPER

Cite this: *RSC Adv.*, 2015, **5**, 92719

Interactions, morphology and thermal stability of graphene-oxide reinforced polymer aerogels derived from star-like telechelic aldehyde-terminal benzoxazine resin†

Almahdi A. Alhwaige,‡*[ab] Saeed M. Alhassan,[c] Marios S. Katsiotis,[c] Hatsuo Ishida*[b] and Syed Qutubuddin*[ab]

Graphene oxide (GO)-reinforced nanocomposite aerogels of polybenzoxazine prepared *via* freeze-drying of GO suspensions in benzoxazine precursor solutions have been studied. The synthesis of GO is confirmed using Raman and Fourier transform infrared (FT-IR) spectroscopy. The benzoxazine monomer (SLTB(4HBA-t403)) has been synthesized using 4-hydroxybenzaldehyde as a phenolic component, paraformaldehyde, and tri-functional polyetheramine (Jeffamine T-403) as an amine source. The chemical structure of the benzoxazine monomer is confirmed by nuclear magnetic resonance (^{1}H-NMR) spectroscopy and FT-IR. The interactions of GO and SLTB(4HBA-t403) have been investigated using FT-IR. The morphological and thermal stability of nanocomposite aerogels are examined and compared with the neat polybenzoxazine aerogel. The structures of the aerogels and the effect of GO on the morphology of the aerogels are studied using X-ray diffraction (XRD), scanning electron microscopy (SEM), and transmission electron microscopy (TEM). The effect of GO on the ring-opening polymerization of benzoxazine is also evaluated using differential scanning calorimetry (DSC) whereas the thermal stability of the nanocomposite aerogels is characterized by thermogravimetric analysis (TGA).

Received 11th August 2015
Accepted 20th October 2015

DOI: 10.1039/c5ra16188f

www.rsc.org/advances

1. Introduction

Aerogels are open-cell porous three-dimensional materials with unusual properties such as ultralow density (0.05–0.1 g cm^{-3}), high surface area, and low dielectric permittivity.[1–4] Since Kistler[1] developed the aerogels in 1931, the sol–gel process has attracted much attention for the fabrication of porous materials.[4] However, active research in this area did not start until about 40 years later.[2] The nano-porous open structure of aerogels is formed by replacing the liquid in a gel with gas during their preparation and persists in the dry state.[2,5,6] The efficiency of cross-linking polymers is expected to produce aerogels with much better properties.[2]

Among the cross-linking polymers, polybenzoxazines have gained much attention as a versatile class of attractive polymeric materials.[7–11] Although the first synthesis of small molecular weight benzoxazine was reported in 1940s,[12] the synthesis and properties of polybenzoxazine derived from monomeric type benzoxazine resins was reported in 1994.[13] More recently, main-chain type cross-linkable polybenzoxazines where the oxazine ring is placed in the main chain have been developed.[14] The development of polybenzoxazine aerogels was first reported in 2009.[15] Meanwhile, several other studies on polybenzoxazine-based polymeric and carbon aerogels containing different monomers have been reported.[6,7,16–20] The advantages of benzoxazine-based nanostructured materials include near-zero shrinkage upon polymerization, excellent thermal stability, and high char yields.[17,21]

Nanocomposite materials are regarded one of the fastest growing fields in the polymer industry.[22] Specific properties of polymeric materials can be enhanced by a uniform dispersion of reinforcement in the polymer matrix, in particular using a small quantity of nanofiller.[23–27] Many different types of fillers, including clay, carbon black, graphene, carbon nanotubes, carbon fibers, and glass fibers have been investigated for producing materials with improved properties. Growing literature about the still-developing field of polybenzoxazine nanocomposites presents major advances that are worthy of consideration. Polybenzoxazine based nanocomposites have attracted the interest of researchers in film form; however,

[a]*Department of Chemical and Biomolecular Engineering, Case Western Reserve University, Cleveland, Ohio 44106-7217, USA. E-mail: aaa148@case.edu; sxq@case.edu*

[b]*Department of Macromolecular Science and Engineering, Case Western Reserve University, Cleveland, OH 44106-7202, USA. E-mail: hxi3@case.edu*

[c]*Department of Chemical Engineering, The Petroleum Institute, United Arab Emiratis*

† Electronic supplementary information (ESI) available: See ESI for experimental details of synthesis and characterizations of GO and SLTB(4HBA-t403), additional FT-IR spectra of SLTB(4HBA-t403)/GO-5% hybrid aerogel. See DOI: 10.1039/c5ra16188f

‡ On leave from Al-Mergib University, Libya, aaalhwaige@elmergib.edu.ly

View Article Online
DOI: 10.1039/C5RA16188F
Paper

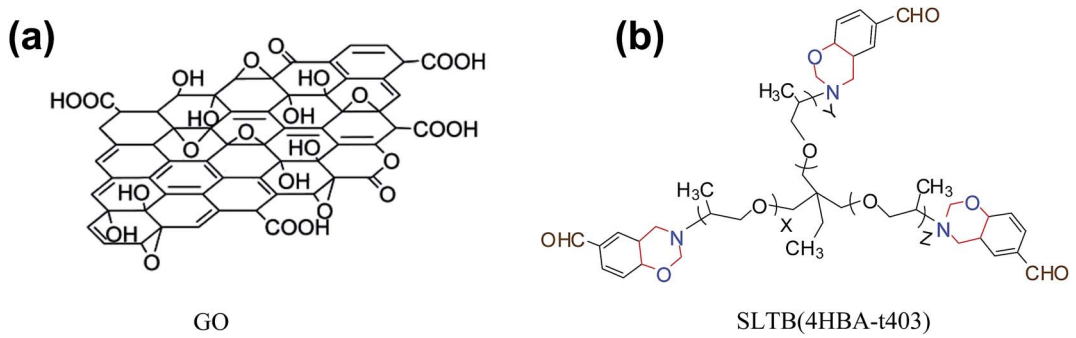

Scheme 1 Chemical structures of: (a) graphene oxide (GO) and (b) the star-like telechelic benzoxazine monomer (SLTB(4HBA-t403)) used in this work.

research in development of polybenzoxazine-based nanocomposite aerogels is limited. Very recently, graphene-reinforced benzoxazine films have been investigated.[28–30] The current study, involves the incorporation of GO into aldehyde-terminal benzoxazine matrix in the form of nanocomposite aerogel, which has not yet been reported.

Graphene nanosheets show unusual enhancement on the properties of nanocomposite materials.[30–32] GO (Scheme 1a) is a layered material produced by the treatment of natural graphite using strong mineral acids and effective oxidizing agents, which introduce a variety of oxygen-based functional groups to the basal planes and edges of graphene layers.[31–37] Graphite is the inexpensive natural source available for production of graphene and GO sheets.[30–34,38] Polymer composites with exfoliated graphite have been reported since 1958.[31] The forces of interaction between the polymers and GO are primarily dipole–dipole interaction and/or hydrogen bonding arising from the polar groups in the polymer and covalent bond formation with the functional groups of hydroxyl (–OH), epoxide (–COC–), and carboxyl (–COOH) on the surfaces of the GO. For example, graphene-based nanocomposite studies were reported using polymers, such as polybenzoxazine,[29,30] polyaniline,[32] polystyrene-polyacrylamide copolymer,[33] poly(allylamine),[39] poly(vinyl alcohol),[40] and epoxy.[41] The development of carbon-based aerogels from graphene and GO have been reported.[42,43]

Combination of benzoxazine and GO is a promising approach to develop the field of benzoxazine nanocomposite aerogels with properties not provided by neat polybenzoxazines. In the current study, a star-like telechelic benzoxazine (Scheme 1b) was used with various GO contents for synthesizing novel nanocomposite aerogels. The morphological and thermal stability of these aerogels have been studied in detail. The novelty of the current study involves our report on the first proposed mechanism of interaction between aldehydes-terminal benzoxazine and GO nanosheets.

2. Experimental section

2.1. Reagents

Graphene oxide (GO) was synthesized from natural graphite powder by modified Hummer's method as previously described.[44,45] Synthesis of GO is described in the ESI, S1.2.† Graphite powder (micro 850) was obtained from Asbury Graphite Mills, Inc. Concentrated sulfuric acid (H_2SO_4, 98%), potassium permanganate ($KMnO_4$ crystal), hydrogen peroxide (H_2O_2, 30% aqueous solution), concentrated hydrochloric acid (HCl) were purchased from Fisher Scientific (USA).

Star-like telechelic benzoxazine was synthesized from 4-hydroxybenzaldehyde (4HBA, 98%, Aldrich Chemicals, USA), polyetheramine (Star-like Jeffamine T-403, M_n = 403 g mol^{-1}, kindly supplied by Huntsman) and paraformaldehyde (96% w/w, Sigma-Aldrich Chemicals, USA) using 1,4-dioxane as solvent. The telechelic is hereinafter abbreviated as SLTB(4HBA-t403). Glacial acetic acid (CH_3COOH), 1,4-dioxane, chloroform, and dimethylsulfoxide (DMSO) were purchased from Fisher Scientific (USA). All chemicals were used without further purification.

2.2. Preparation of SLTB(4HBA-t403)/GO nanocomposite aerogels

New nanocomposite aerogels were prepared *via* freeze-drying of various GO suspensions in SLTB(4HBA-t403) solutions (Fig. 1). Samples are abbreviated as SLTB(4HBA-t403)/GO-*x* where *x* is the various GO content of 0, 3, 5, and 10 wt%. The starting precursor of benzoxazine (SLTB(4HBA-t403)) was prepared by our previously reported method[46] and can be found in the ESI, S1.3.† The preparation of the aerogels will be presented using SLTB(4HBA-t403)/GO-5% as an example of nanocomposite aerogel containing 5 wt% GO. Specifically, 0.05 g of GO were dispersed in 10 mL of DMSO, while at the same time, 0.95 g of SLTB(4HBA-t403) were dissolved in 10 mL of DMSO using a magnetic stirrer at ambient conditions. After completely dissolving SLTB(4HBA-t403), the solution was added slowly to the GO colloidal suspension under vigorous agitation using a mechanical stirrer at 1000 rpm at room temperature. The mixing lasted for 3 h, after which the mixture was sonicated for 30 min. Then, the collected suspension was transferred into glass vials, sealed, and then heated slowly to 125 °C in an oven for 24 h. The attained nanocomposite product was partially cross-linked due to ring-opening polymerization of benzoxazine precursor.[15] The collected colloidal suspension was frozen using ethanol and solid carbon dioxide at −70 °C and ambient

View Article Online
DOI: 10.1039/C5RA16188F
RSC Advances

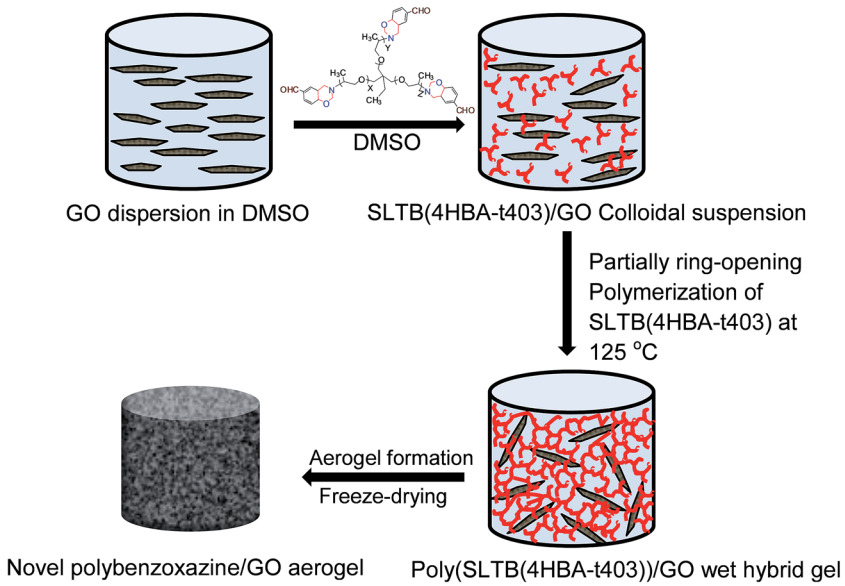

Fig. 1 Illustration of preparation process for novel polybenzoxazine/GO nanocomposite aerogels.

pressure. Finally, the frozen poly(4HBA-t403/GO-x) suspension was transferred to a VirTis AdVantage@EL-85 freeze-drier for five days. Aerogels were obtained after drying the frozen solvent by sublimation under high vacuum conditions.

2.3. Cross-linking and carbonization of the aerogels

The resulting aerogels were thermally treated at 150 °C, 175 °C, and 180 °C for 2 h to obtain the fully polymerized and cross-linked polybenzoxazine nanocomposite aerogels (Scheme 2). The polymerized aerogels were carbonized under nitrogen flow of 60 mL min^{-1} and a temperature ramp rate of 10 °C min^{-1} from ambient temperature to 900 °C.

2.4. Characterization

Micro-Raman scattering studies were carried out at room temperature using a Horiba Jobin-Yvon LabRam HR800 spectrometer which is equipped with a charge coupled detector and two grating systems (600 and 1800 lines per mm). A HeNe laser ($\lambda = 632.8$ nm), with an optical power of 17 mW and a spot size of 1 μm^2, was focused on the sample with an Olympus microscope. Raman shifts were calibrated with a Si (100) wafer using the 520 cm^{-1} peak.

X-ray diffraction (XRD) was used to determine the increment of the d-spacing in the GO sheets through intercalation of the cationic organic. X-ray diffractograms of the aerogels were obtained by Cu-Kα radiation ($\lambda = 0.15418$ nm) with scanning rate of 0.2 degrees min^{-1} at room temperature. XRD is performed on dried thin film of aerogels. The aerogel samples were cut into thin disks prior to X-ray measurements. Bragg's equation, $\lambda = 2d \sin(\theta)$ where d is the layer spacing and θ is the angle of diffraction, was used to compute the d-spacing for GO nano-sheets.

Fourier-transform infrared (FT-IR) spectroscopy was used to investigate the oxidation of graphene, polymerization of benzoxazine and the interactions between benzoxazine and GO. FT-IR spectra were obtained using a Bomem Michelson MB-100 FT-IR spectrometer with a dry air purging unit and a deuterated triglycine sulfate detector at a resolution of 4 cm^{-1}.

Textural morphology of the aerogels was observed with Scanning Electron Microscopy (SEM) and Transmission

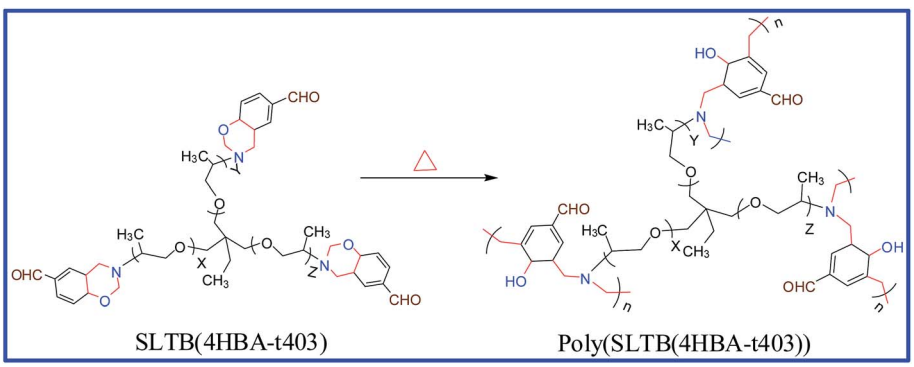

Scheme 2 Thermally accelerated synthesis of poly(SLTB(4HBA-t403)) from its precursor.

View Article Online
DOI: 10.1039/C5RA16188F
Paper

Electron Microscopy (TEM). SEM analysis was performed with a FEI Quanta 250 (FEG), coupled with Energy Dispersion X-ray Spectroscopy (EDS). Regarding sample preparation, a thin slice (~1.5 mm) cut on the vertical axis of each of the cylindrically shaped specimens was mounted on standard aluminum SEM stabs using conductive silver glue. TEM analysis was performed with a FEI Tecnai G20, coupled with EDS and a Gatan GIF 963 energy filtered camera. Samples were crushed using a mortar and pestle and then dispersed in high purity ethanol (99.99%) in an ultrasonic bath for ~30 s. A drop of the dispersed phase would be deposited on Cu grid covered with a thin layer of amorphous carbon (lacey carbon), following which the grid would be immediately transferred to the TEM holder to avoid contamination.

The apparent bulk density (ρ_b) of the aerogel was obtained from the aerogel mass (m) and its volume (V) as described in eqn (1)

$$\rho_b = \frac{m}{V} \quad (1)$$

The values of skeletal density (ρ_s) were obtained by using helium in gas-displacement pycnometer. The apparent porosity percentage of the aerogels was calculated according to the following relation.[44]

$$\text{Porosity}\% = \left(1 - \frac{\rho_b}{\rho_s}\right) \times 100 \quad (2)$$

The thermal stability of the aerogels were evaluated by thermogravimetric analysis (TGA) and differential thermogravimetric analysis (DTGA) using a TA Instruments High Resolution 2950. A sample (5–10 mg) from each obtained aerogel was placed in a platinum pan and heated from room temperature to 900 °C at a temperature ramp rate of 10 °C min^{-1} under nitrogen atmosphere with a gas flow rate of 60 mL min^{-1}.

3. Results and discussion

3.1. Preparation of graphene oxide (GO)

The oxidation of graphite has been confirmed by Raman spectroscopy and FT-IR. As shown in Fig. 2, the Raman spectrum of natural graphite exhibits strong lines at 1577 cm^{-1} and 2685 cm^{-1}, which are assigned to the G band and 2D band, respectively, while the D band is shown as a weak band at 1328 cm^{-1}.[39,47,48] The two most intense lines appearing at 1597 and 1330 cm^{-1} for GO correspond to the G and D bands, respectively.[34] As shown in the GO spectra, the D band shifts to higher frequency and becomes prominent. The ratio of D to G band intensity (I_D/I_G) equals to 1.27, indicating the reduction in the average size of sp^2 domains due to extensive oxidation.[34,48]

FT-IR results confirm the introduction of oxygen-based functional groups on the basal plane and edge of graphene (ESI, Fig. S1†). Expectedly, there is no significant peak found in the natural graphite spectrum, while the spectrum of GO shows characteristic band at 3380 cm^{-1} (the OH stretching mode), 1720 cm^{-1} (the C=O stretching mode of carboxylic acid groups), 1209 cm^{-1} (=C–OH stretching vibrations) and 1043 cm^{-1} (C–O stretching vibrations). These results are in agreement with reported literature.[34–37]

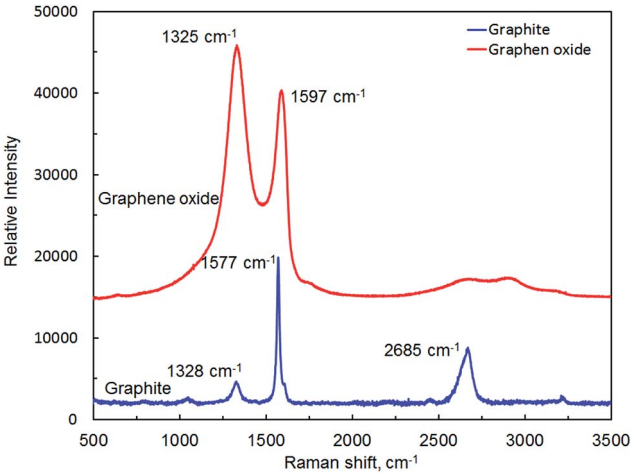

Fig. 2 Raman spectra of graphite (lower spectrum) and GO (upper spectrum).

3.2. Interactions of GO and polybenzoxazine

Recently, much attention has focused on the development of polybenzoxazine-based nanocomposite materials.[29,30] However, interaction of GO with benzoxazine containing functional groups have not yet been reported. GO contains several reactive moieties on the surface of its nanosheets including epoxide, hydroxyl, and carboxyl groups.[34,36,41] The interactions between benzoxazine and epoxy during the polymerization have been investigated.[49,50] Jubsilp *et al.*[50] reported that DSC thermograms of benzoxazine/epoxy blends showed at least two possible reactions: (i) the exothermic peak due to polymerization of benzoxazine monomers. Phenolic structure is an initiator and catalyst for polymerization of both benzoxazine[49–51] and epoxy.[52] (ii) The reaction between the epoxide groups on the epoxy with the phenolic hydroxyl groups on polybenzoxazine. Accordingly, we suggest that epoxy groups on the surface of GO sheets attach the polybenzoxazine structure during the polymerization step. Furthermore, hydrogen bonding between the polar groups on both polybenzoxazine and GO may take place. The proposed interactions between SLTB(4HBA-t403) as aldehyde-terminal benzoxazine and GO are shown in Schemes 3 and 4, while FT-IR was used to confirm these interactions.

The structure of SLTB(4HBA-t403) benzoxazine monomer was confirmed with ^{1}H-NMR and FT-IR as shown in the ESI Fig. S2 and S3,† respectively; detailed discussion can be found in S2.2.† FT-IR was used to study the polymerization behaviour of SLTB(4HBA-t403)/GO nanocomposite aerogels. A typical FT-IR profiles of neat SLTB(4HBA-t403) at 75 °C and SLTB(4HBA-t403)/GO-5% aerogel at various temperatures (60, 160, 200 and 900 °C) are shown in the ESI, Fig. S4.† FT-IR spectrum of pristine GO (ESI, Fig. S1†) indicates that the hydroxyl functional groups on the surface of graphene sheets have characteristic band at 3380 cm^{-1} (the OH stretching mode). FT-IR results of SLTB(4HBA-t403) (ESI, Fig. S4a†) reveals that there is no

View Article Online
DOI: 10.1039/C5RA16188F
RSC Advances

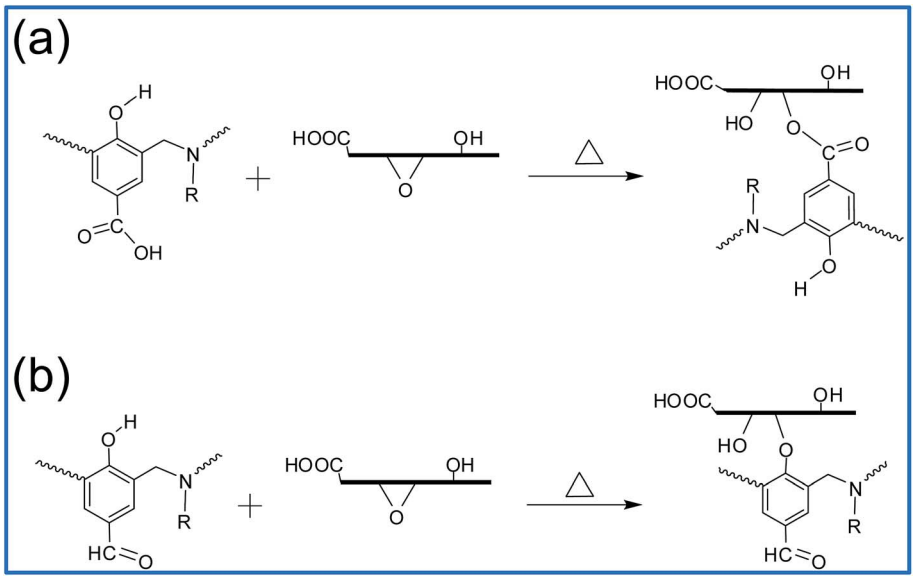

Scheme 3 Proposed chemical interaction between SLTB(4HBA-t403) and GO: (a) esterification-based on carboxylic acid of oxidized aldehyde-functional benzoxazine and (b) etherification-based on the residual aldehyde-functional benzoxazine.

absorption bands in the range 3400–3000 cm^{-1}. After dispersion of GO in SLTB(4HBA-t403) matrix, a broad band appearing at 3465 cm^{-1} indicates the presence of hydroxyl functional groups (–OH) of GO.[34] The frequency shift from 3380 cm^{-1} to 3465 cm^{-1} is likely due to the weakening of OH hydrogen bonds caused by the more hydrophobic environment of GO surrounded by SLTB(4HBA-t403), which is consistent with the exfoliated GO. The samples heated at higher temperatures show more absorption intensities of this peak due to the newly created phenolic –OH groups in the polybenzoxazine chains. The phenolic hydroxyl group is also confirmed by the appearance of new absorption peak around 3300 cm^{-1}.[7]

From the ESI Fig. S4,† it is obvious that the characteristic bands of the GO functional groups heavily overlap with this newly generated OH band and it makes difficult to study the interaction of GO and benzoxazine by FT-IR. The problem is compounded by the low concentration of GO compared to the amount of polybenzoxazine matrix in all studied samples. Therefore, further experiments were performed to confirm SLTB(4HBA-t403)/GO interactions. The investigation of interfacial interactions between SLTB(4HBA-t403) and GO were evaluated by FT-IR using sample with high concentration of GO (SLTB(4HBA-t403)/GO is 40/60 weight percent), which forms a thin-layer of SLTB(4HBA-t403) on GO nanosheets.

The sample was prepared by blend of a concentration of benzoxazine (40 wt%) and GO (60 wt%) and thoroughly mixed for one min. The solution was casted on KBr pellet and dried at room temperature for FTIR measurements. Then, the casted film was subjected to a ring-opening polymerization of benzoxazine monomer schedule of 2 h at each 100, 125, 175 °C.

Fig. 3 shows FT-IR spectra of neat GO, neat SLTB(4HBA-t403), and treated SLTB(4HBA-t403)/GO nanocomposite at various temperatures. The FT-IR characteristics of GO are separately discussed in detail (ESI, Fig. S1†). The important characteristic infrared absorptions of the neat SLTB(4HBA-t403) structure are clearly observed as discussed (ESI, S2.2 and Fig. S3†). The FT-IR spectrum of adsorbed layer of SLTB(4HBA-t403) on GO sheets (Fig. 3c) shows a characteristic absorption band at 1728 cm^{-1}, which is attributed to the C=O stretching band of carboxylic acid-functional groups of GO.[34,53] This peak slightly changed with heat treatment due to functional groups attached to the carbonyl with a benzene ring or double bond in conjugation with carbonyl.[54] The results in Fig. 3c reveal that mixing of GO to SLTB(4HBA-t403) significantly shifts the absorption band at 1114 cm^{-1} of polyether chain to lower wavenumber due to hydrogen bonding with the adsorbed water on the GO-functional groups. After thermal treatment from 100 °C up to 175 °C, this band returned to the same position (Fig. 3b) due to the evaporation of moisture.

Moreover, the ester-linkage formation in benzoxazine/epoxy resin blend system has been reported.[49] The characteristic FT-IR bands of epoxy band (around 950–900 cm^{-1}) overlap with the absorption bands of benzoxazine, making it difficult to follow the disappearance of epoxy bands upon polymerization. However, the observation of the relative increase in the band at 1728 cm^{-1} is due to ester group formation. More recently, chemical interaction of GO with phenolic resin has been reported.[55] Zhou *et al.*[55] documented that esterification reaction occurred between hydroxyl groups (–OH) on resole and carboxyl groups (–COOH) on GO, as confirmed by the absorption band at 1722 cm^{-1}. Therefore, herein, the absorption band at 1728 cm^{-1} is attributed to the esterification reaction between phenolic –OH and carboxylic groups of GO after heat treatment. In addition, the absorption bands at 2333 and 2364 cm^{-1} are assigned to CO_2 as a result of the oxidation of aldehyde groups.[56] In aldehyde-functional benzoxazines, oxidation of aldehyde groups to form carboxylic groups has been reported.[56]

View Article Online
DOI: 10.1039/C5RA16188F
Paper

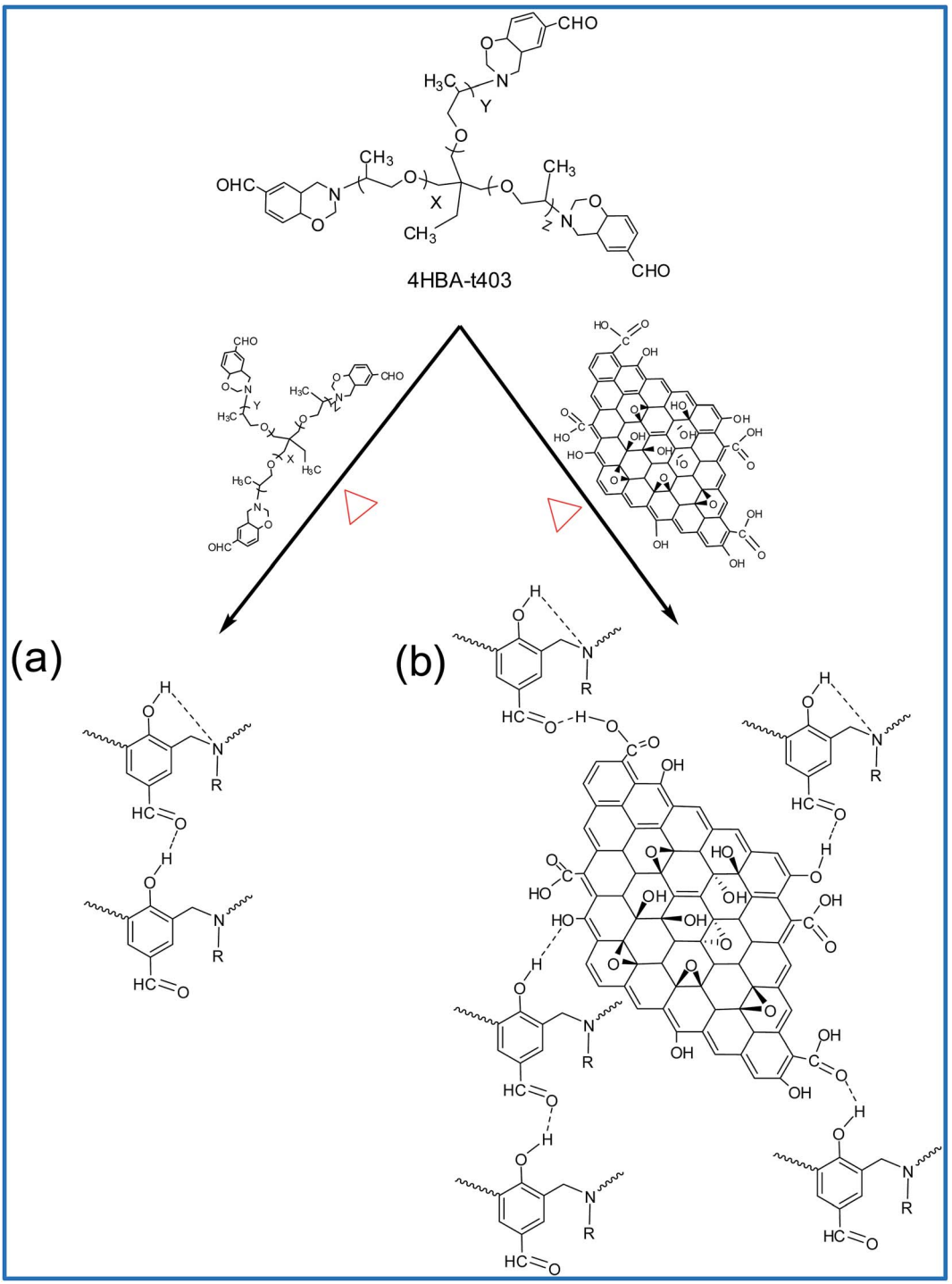

Scheme 4 Proposed hydrogen bonding network formed between oxygen-functionality on GO and SLTB(4HBA-t403): (a) hydrogen bonding in polymerized aldehyde-functional benzoxazine [adapted from ref. 56] and (b) hydrogen bonding in polymerized SLTB(4HBA-t403)/GO.

Therefore, ester formation resulting from carboxylic groups-epoxy reaction possibly occurred as seen in Scheme 3a. In this case of oxidation of aldehyde groups, the released CO_2 would present a great advantage to partially contribute to the porous structure of the aerogels, further investigation will be discussed in details elsewhere.[57]

Furthermore, during heat treatment of ring-opening polymerization of benzoxazine, the produced phenolic hydroxyl is proposed to react with epoxy groups of GO (etherification). The polyether band at 1114 cm^{-1} became a broader peak and overlapped with 1161 cm^{-1}, which attributed to the chemical attachment of polybenzoxazine with GO *via* phenolic hydroxyl-epoxy reaction as proposed in Scheme 3b. The resulting

View Article Online
DOI: 10.1039/C5RA16188F
RSC Advances

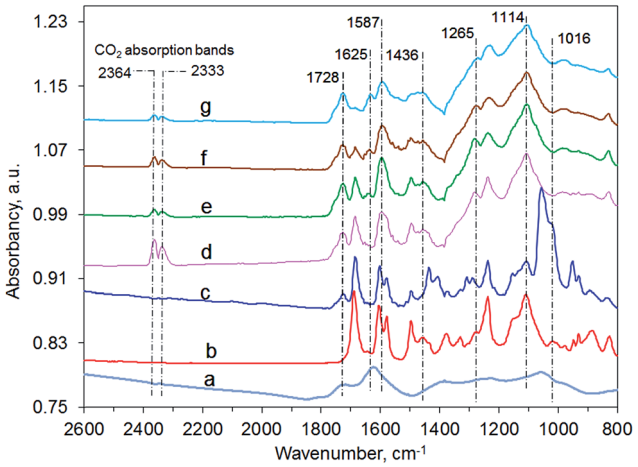

Fig. 3 FT-IR spectra of interfacial interaction of GO and SLTB(4HBA-t403): (a) neat GO, (b) neat SLTB(4HBA-t403), (c), (d), (e), and (f) SLTB(4HBA-t403)/GO (40/60 weight percent) at 25, 100, 125, and 175 °C, respectively.

absorption band increased with increasing heat treatment due to production of phenolic hydroxyl groups (–OH). The absorption bands in the range 1608–1583 cm^{-1} in the FT-IR spectra of SLTB(4HBA-t403)/GO nanocomposites become overlapped bands due to newly appeared C=C band from thermal treatment of GO.[30] Heat treatment of GO partially decomposes the functional groups resulting in aromatic conjugated bonds of graphene.

Hydrogen bonding is possible between the aldehyde-functional benzoxazines and GO formed. Polybenzoxazines contain extensive intermolecular and intramolecular hydrogen bonding between phenolic hydroxyl –OH and electronegative atoms such as O and N.[7,56,58–60] Also, hydrogen bonding interaction between the aldehyde groups and polybenzoxazine has been reported as seen in Scheme 4a.[56] In the polymerized aldehyde-functional benzoxazine monomer, the aldehyde groups contain electronegative O atoms, which can form intermolecular hydrogen bonding with H atoms of phenolic hydroxyl groups. Herein, the H atoms of hydroxyl groups of GO may show similar tendency (Scheme 4b). Fig. S5† shows the infrared spectra of the C=O stretching (aldehyde groups) of SLTB(4HBA-t403) and SLTB(4HBA-t403)/GO samples. The neat SLTB(4HBA-t403) gives a carbonyl absorption peak at 1688 cm^{-1} (Fig. S5b†).[56,58,59] After adding the GO into the SLTB(4HBA-t403) system (Fig. S5c†), the carbonyl stretching frequency is shifted into 1683 cm^{-1}, corresponding to the hydrogen bonded aldehyde groups of SLTB(4HBA-t403) with functional groups on GO sheets as described in Scheme 4b. This new band (1683 cm^{-1}) gradually shifts into the hydrogen bonded carbonyl (1633 cm^{-1}) with increasing heat treatment of nanocomposite sample (SLTB(4HBA-t403)/GO).[58] These results suggest that there interaction in the residual aldehyde groups of polybenzoxazine resins. These results are in agreement with literature.[56] As seen in Fig. S5,† the existence of hydrogen bonding makes the frequency of the C=O band (1683 cm^{-1}) decrease in the FT-IR spectrum. The hydrogen bonding results from the interaction of electronegative atoms in the residual aldehyde groups with H atoms of hydroxyl groups of both GO and polybenzoxazine. Also, the phenolic hydroxyl groups of polybenzoxazine may form hydrogen bonding with hydroxyl groups of GO. Further hydrogen bonding may occur between carboxylic groups of GO and H atoms of polybenzoxazine (–OH and –COH). According to these results, one can conclude that polymerized SLTB(4HBA-t403)/GO contains a large amount of intermolecular hydrogen bonding formed by residual aldehyde and phenolic hydroxyl groups with oxygen-functional groups of GO (Scheme 4). Adhikari[61] *et al.* reported that functional groups (–OH, –COOH) are able to form hydrogen bonds with other molecules under appropriate conditions. As result of hydrogen bonds, polymers can be assembled with GO to form a hydrogel matrix.[43,62]

To conclude the FT-IR results, incorporation of neighboring group of aldehyde moieties in benzoxazine monomers play a role for providing more interaction sites during hybridization of polybenzoxazine with GO. These interactions contribute to the enhanced performance of the aerogels as a new class of nanocomposite aerogels. The strong interaction of benzoxazine chains with GO nanosheets leads to high performance nanocomposites-based materials.

3.3. X-ray diffraction analysis (XRD)

Fig. 4 displays the X-ray diffractograms of graphite, GO, and the nanocomposite aerogels. In the case of oxidation of the neat graphite, the d_{002} diffraction peak in the natural graphite shifted from around $2\theta = 26°$ to lower 2θ values, indicating the GO formation.[34,36,38,63]

The results show that the *d*-spacing of graphene layers was increased from 0.34 nm to 0.83 nm after the oxidation process due to the formation of oxygen-functional moieties which are acting as spacers. The challenges are to achieve molecule-level dispersion and maximum interfacial interaction between the nanofiller and the polymer matrix at low loading. The XRD

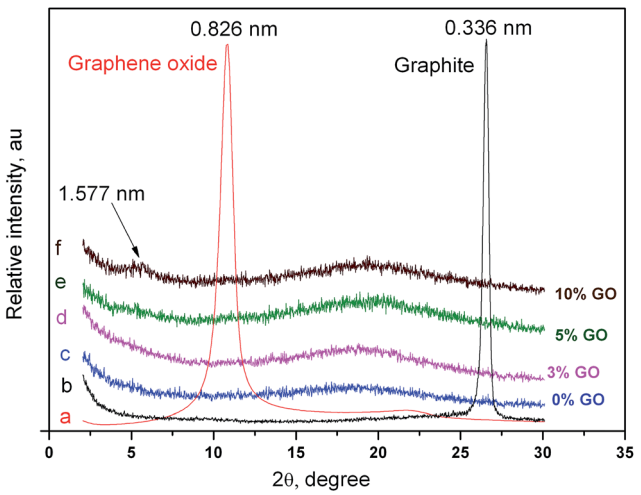

Fig. 4 XRD diffractograms of profiles of: (a) GO, (b) graphite, (c), (d), (e), and (f) of SLTB(4HBA-t403)/GO nanocomposites with various GO contents of 0 wt%, 3 wt%, 5 wt%, and 10 wt% GO, respectively.

View Article Online
DOI: 10.1039/C5RA16188F
Paper

pattern of neat SLTB(4HBA-t403) (Fig. 4c) shows a typical diffraction of an amorphous polymer with a broad peak at $2\theta = 18°$. In the case of SLTB(4HBA-t403)/GO aerogels, the effect of SLTB(4HBA-t403) on exfoliation of GO also has been evaluated. Up to 5 wt% of GO, no obvious diffraction peak is seen below $2\theta = 10°$. This means that GO may be fully exfoliated in polybenzoxazine matrix due to the strong interaction between GO and SLTB(4HBA-t403), although the concentration of GO is so low and verification of complete exfoliation only by XRD is difficult. However, the aerogel containing 10 wt% GO shows a broad diffraction peak at $2\theta = 5.6°$, indicating that polybenzoxazine has intercalated fraction of GO. Observation of intercalated fraction implies the trend to aggregate the nanoparticles starts around this concentration. As a result of polybenzoxazine intercalation, the *d*-spacing of GO increased from 0.826 nm to 1.58 nm.

3.4. Morphological and microstructure analysis of GO reinforced aerogels

Effects of hybridization of SLTB(4HBA-t403) matrix with GO on morphology and structure of benzoxazine aerogel have been investigated. The density and porosity of all obtained aerogels are summarized in Table 1. Slightly differences were observed in physical structures of neat and nanocomposite polybenzoxazine aerogels. The apparent density (ρ_b) and porosity of the obtained aerogels are in the range of 0.1482–0.1550 g cm^{-3} and 84.50–86.52%, respectively. These results confirmed highly porous structure of the hybrid aerogels.[44] The results indicated that bulk density (ρ_b) of neat polybenzoxazine aerogel is higher than the nanocomposite aerogels, which can be related to their microstructures behavior as shown in Fig. 5. By comparing SEM micrographs for the neat polybenzoxazine and nanocomposite aerogel (SLTB(4HBA-t403)/GO-5%), samples containing GO have more overlapping layers in the morphology than GO-free aerogels. This increase in the number of layers may lead to the observed increase in the porosity with increasing GO content.

3.4.1. Scanning electron microscopy (SEM). The morphology of polybenzoxazine aerogels has been reported earlier.[13,15] To the best of our knowledge, this is the first time reported in literature where morphology and microstructure of polybenzoxazine/GO aerogels is studied with SEM. SEM analysis shows that all samples contain a highly porous structure, a result of solvent removal; however, pore sizes do not exhibit uniform distribution. The cross section of the polybenzoxazine aerogel is shown in Fig. 5a and b. The cross section of the specimen containing 5% GO (SLTB(4HBA-t403)/GO-5%) is shown in Fig. 5c and d, while lateral sections are shown in Fig. 5e–g.

Table 1 Bulk density and porosity of the obtained aerogels

Sample code	Bulk density (g cm^{-3})	Porosity (%)
SLTB(4HBA-t403)/GO-0%	0.1550	84.50
SLTB(4HBA-t403)/GO-1%	0.1475	85.38
SLTB(4HBA-t403)/GO-3%	0.1477	85.65
SLTB(4HBA-t403)/GO-5%	0.1478	85.91
SLTB(4HBA-t403)/GO-10%	0.1482	86.52

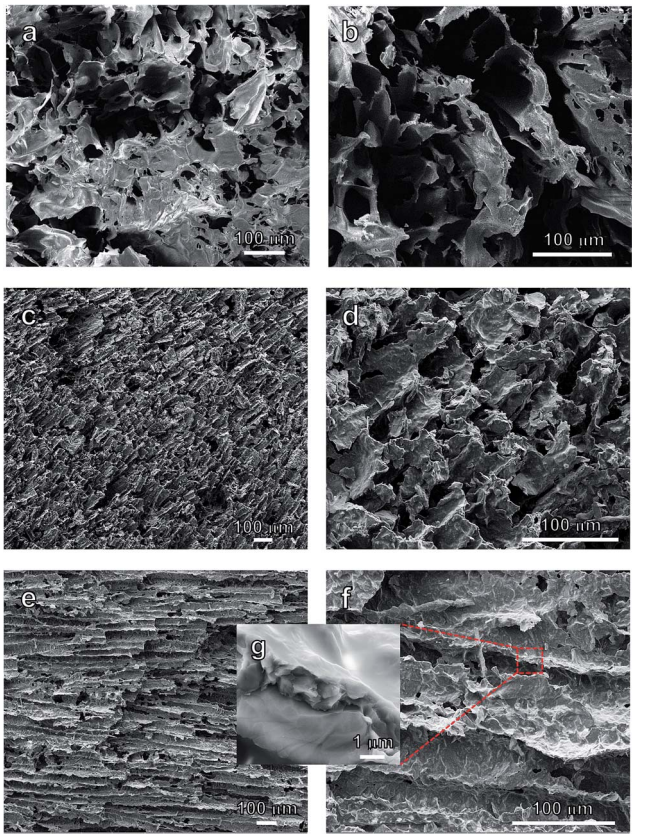

Fig. 5 SEM micrographs of polybenzoxazine-based aerogels at various microscope magnifications: (i) cross-section images of polymeric aerogel without GO: (a) and (b). (ii) SLTB(4HBA-t403)/GO-5% aerogel: (c) and (d) cross-section, (e) and (f) lateral-section; (g) inset shows the fractured structure of the layer separating two aerogel pores.

It is clear that the pore structure of nanocomposite aerogels is different than that of the organic aerogel as the pore sizes in polymeric aerogel (Fig. 5b) appear larger than those of the GO reinforced aerogel (Fig. 5d). The structure of pores is dependent on the size of the ice crystals during the fabrication of the aerogels. During the freezing, as the ice crystals grow, microribbons form on the walls of the aerogel.[1,45] The small size of ice crystal growth leads to narrow pore, resulting in an increase in the surface area. In addition, the GO reinforced aerogels exhibit a more layered structure than the polymeric aerogel as shown by SEM images of lateral sections (side view) of the 5% GO reinforced aerogels (Fig. 5e–g). Furthermore, it is clearly seen that the surface of the layers exhibits increased roughness.[1] In addition, the layers extend through the length of the aerogel and connected together *via* strands to create irregular pores. Fig. 5g illustrates the morphology of the fractured structure of edge between two aerogel pores at high magnification (×40 000 and scale of 3 μm). The inner surface of the fracture is very different from that of the outer surface due to the presence of the nanofiller. It is interesting to note that the

View Article Online
DOI: 10.1039/C5RA16188F
RSC Advances

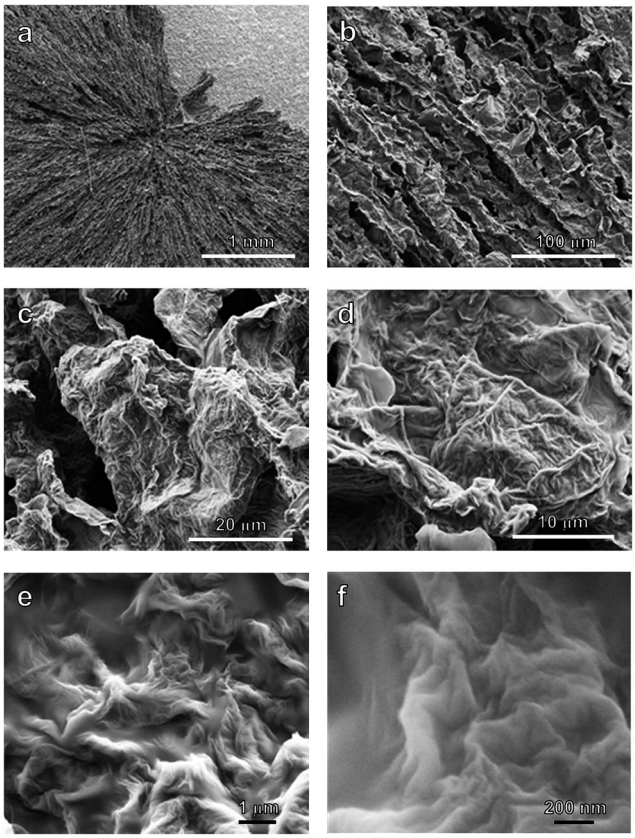

Fig. 6 SEM micrographs of poly(SLTB(4HBA-t403)/GO-5%) carbon aerogels at different microscope magnifications.

center area shows rough appearance with what appears as a hierarchical structure, while the GO is distributed on the interior surface of the layer without any aggregation.

Carbon aerogels possess large surface area, which have advantages in catalysis and adsorption applications[64] as well as electrodes for supercapacitors.[16] Morphological behavior of carbon aerogels has been extensively studied using SEM.[16,42,43] Polybenzoxazine-based carbon aerogels and xerogels have been investigated.[16,17] Herein, morphology of carbon neat polybenzoxazine and polybenzoxazine/GO nanocomposites aerogels studied. Fig. 6 contains the SEM micrographs of carbonized SLTB(4HBA-t403)/GO-5% aerogel. Fig. 6b reveals that the surface layers become coarser after carbonization. The high magnification SEM images (Fig. 6c–e) show surface topology becomes irregularly wrinkled upon carbonization.

The possible contribution to these wrinkles may be the crumpling of graphene nanosheets that result from the reduced GO and after the decomposition of soft segments of polybenzoxazine. Therefore, random distribution of GO sheets can be observed (Fig. 6f). The observations made with SEM are in good agreement with XRD results which show that GO is highly exfoliated in the polymeric matrix.

3.4.2. Transmission electron microscopy (TEM). The structure and morphology of as-prepared polybenzoxazine/GO aerogels were also investigated by means of transmission electron microscopy (TEM). TEM images of the neat poly(SLTB(4HBA-t403)) are shown in Fig. 7, while TEM images of polymerized and carbonized SLTB(4HBA-t403)/GO-5% aerogels are shown in Fig. 8 and 9 respectively. As seen in Fig. 7, TEM analysis revealed the wide distribution of size and shape observed for the pores of the polybenzoxazine aerogel. Furthermore, the amorphous nature of the specimen was confirmed with Selected Area Electron Diffraction (SAED) and High Resolution TEM (HRTEM). Similar finds have been previously reported for neat polybenzoxazine-based porous carbons.[16,17] EDS analysis showed minor presence of Cl impurities (>0.1%).

Fig. 8 shows TEM micrographs of SLTB(4HBA-t403)/GO-5% polymerized aerogel. Concerning the polymerized SLTB(4HBA-t403)/GO-5% aerogel, its morphology is similar to the polybenzoxazine aerogel, exhibiting a wide distribution of pore size and shape. Thin carbon layered structures with no aggregation of GO were observed, as expected from previous work by Alhassan *et al.*[30] Overall, the GO sheets were found to be homogeneously dispersed into the polybenzoxazine amorphous structure. Similar finds are observed for the carbon aerogel containing 5 wt% GO, although in this case the ordering of the GO sheets appeared to be higher; this was observed with HRTEM analysis at the edge of particles, where turbostratic and graphitic layers were observed (see Fig. 9b).[65]

A strong indication of the increased GO presence was provided with EELS analysis, shown in Fig. 10. Specifically, carbon hybridization was evaluated by acquiring the C K-edge

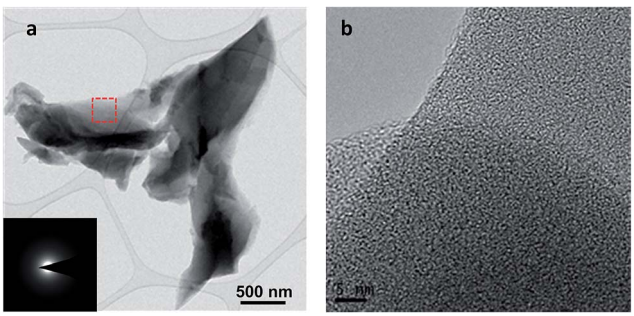

Fig. 7 TEM (a) and HRTEM (b) images of poly(SLTB(4HBA-t403)) aerogel; inset: SAED pattern (collected at area marked with red rectangle) reveals no crystalline structure.

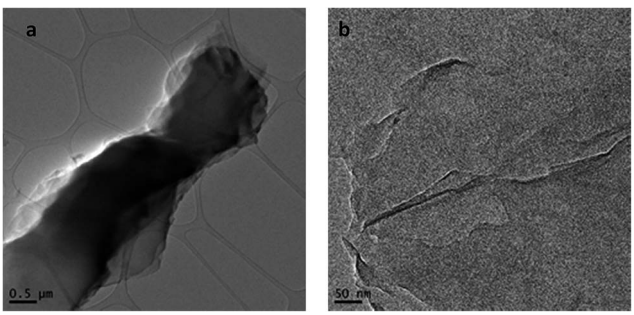

Fig. 8 TEM images of SLTB(4HBA-t403)/GO-5% polymerized aerogel; (a) low magnification, (b) high magnification.

View Article Online
DOI: 10.1039/C5RA16188F
Paper

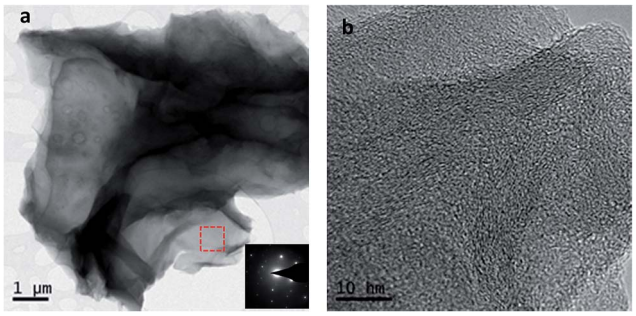

Fig. 9 TEM images of SLTB(4HBA-t403)/GO-5% carbon aerogel: (a) low magnification, (b) high magnification; inset: SAED pattern (collected at area marked with red rectangle) reveals an exist crystalline structure due to presence of GO.

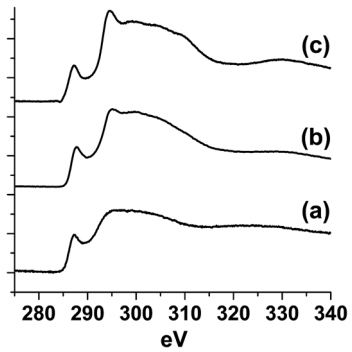

Fig. 10 Background subtracted and deconvoluted EELS spectra at carbon K-edge for poly(SLTB(4HBA-t403)) aerogel (a), SLTB(4HBA-t403)/GO-5% polymerized aerogel (b) and SLTB(4HBA-t403)/GO-5% carbon aerogel (c).

for the three specimens mentioned above: poly(SLTB(4HBA-t403)) aerogel, SLTB(4HBA-t403)/GO-5% polymerized aerogel and SLTB(4HBA-t403)/GO-5% carbon aerogel. The characteristic peaks corresponding to sp^2 hybridization (1s → π* at 284 eV and 1s → σ* at 291 eV) are more prevalent in the carbonized and polymerized aerogels, due to GO presence in the matrix. On the other hand, the polybenzoxazine aerogel exhibits significantly lower sp^2 hybridization, which is mostly attributed to its amorphous nature.

The overall of microstructure analysis can be summarized as the GO sheets were found to be homogeneously distributed into the polybenzoxazine aerogels. In addition, GO enhances the microstructure and reduces the pore size of polybenzoxazine aerogels, while the surface topology of GO/polybenzoxazine aerogel becomes irregularly wrinkled upon carbonization due to the unique structure of GO.

3.5. Effect of GO on polymerization behavior of benzoxazine monomer

The influence of GO content on the polymerization behavior of benzoxazine monomer was monitored and analyzed by DSC. As seen in Fig. 11, the heat treatment of neat SLTB(4HBA-t403) and pristine GO showed only one exothermic peak at 207 and

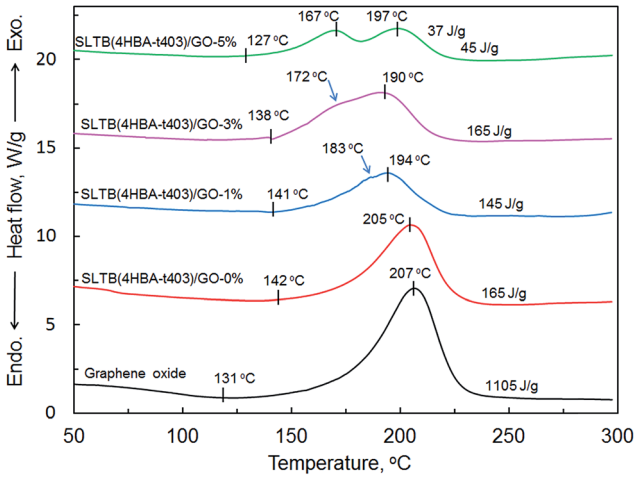

Fig. 11 DSC thermograms of SLTB(4HBA-t403)/GO aerogels with different GO content.

205 °C, respectively. The similarity of these two maxima is purely accidental. On the other hand, SLTB(4HBA-t403)/GO aerogels showed multiple overlapped or separated exothermic peaks with lower onset temperatures. This observation suggests that polymerization pathway of SLTB(4HBA-t403)/GO nanocomposites is different comparing with the neat SLTB(4HBA-t403). This is hypothesized to be due to the catalytic effect caused by the surface species of GO.

It has been reported that both phenolic and carboxylic groups exist on the GO surface.[66] Also, both phenolic and carboxylic acids are effective benzoxazine polymerization initiators and/or catalysts.[51,67] As a result, increase in the GO contents decreases the onset polymerization temperature of the SLTB(4HBA-t403)/GO aerogels. The recent report by Gu *et al.*[29] demonstrated that GO has a catalytic effect on the ring-opening polymerization of benzoxazine; however, their DSC investigation did not show de-oxygenation peak of GO. On the other hand, the exothermic peak of GO at 207 °C observed in this study is in agreement with reported results.[60,68] Zhao *et al.*[63] found that de-oxygenation of GO has a large single exothermic peak at 200 °C. Furthermore, Alhassan *et al.*[30] reported two exothermic peaks for benzoxazine/GO nanocomposites. It is noteworthy to mention that presence of GO in all cases has catalytic effect on the ring-opening polymerization of the benzoxazine monomer. The results in Fig. 11 reveal that the maximum temperature of the polymerization exotherm on DSC and the area under the peak are significantly shifted to lower values. As an example, 5 wt% GO the onset temperature and maximum temperature of neat SLTB(4HBA-t403) decreased from 142 and 207 °C to 127 and 167 °C, respectively, indicating that GO has significant catalytic activity on benzoxazine polymerization.

DSC results also show that addition of GO to benzoxazine matrix has catalytic effect on reducing the polymerization enthalpies of aldehyde-terminal benzoxazine monomer. Neat aldehyde-terminal benzoxazine and GO show exotherm with enthalpies of 165 and 1105 J g^{-1}, respectively. Accordingly, for

View Article Online
DOI: 10.1039/C5RA16188F
RSC Advances

instant, theoretical values of enthalpies for benzoxazine polymerization of samples containing 1% and 3% of GO should read 174 and 193 J g^{-1}, respectively. However, the DSC results indicated that the polymerization enthalpies of same nanocomposite samples are 145 and 165 J g^{-1}, respectively.

3.6. Thermal stability of GO reinforced aerogels

Polybenzoxazine-based porous materials including aerogels exhibit anomalous thermal stability.[6,15,17] Lorjai *et al.*[6] studied the thermal decomposition of neat polybenzoxazine in comparison to the corresponding aerogel. Polybenzoxazine aerogel exhibited a much higher degradation temperature and char yield than the corresponding bulk polybenzoxazine. Thermal stability of the obtained aerogels after polymerization was evaluated by TGA and DTG. TGA profiles of pristine GO, poly(SLTB(4HBA-t403)) aerogel, and poly(SLTB(4HBA-t403)/GO) aerogels are shown in Fig. 12 and the results are summarized in Table 2. The results indicate that the poly(SLTB(4HBA-t403)/GO) has weight loss at lower temperature than the neat poly(SLTB(4HBA-t403)) due to the low temperature weight loss of GO; however, the char yield is higher with GO because of the higher char yield of GO than polybenzoxazine. TGA results of GO show two regions of weight loss. The first weight loss occurred below 100 °C, which is due to the evaporation of the adsorbed moisture. The second weight loss is ascribed to the decomposition of functional groups.[63]

The results in Table 2 indicated that the maximum degradation temperature of neat GO is 211 °C, which is much lower than that for the neat polybenzoxazine. The lower degradation temperature is attributed to the low thermal stability of soft segment of the functional groups of GO. This investigation is in agreement with literature. The previous studies reported that the thermal decomposition of instable oxygen-containing functional groups occurring at a temperature of 200 °C.[34] The TGA results showed that stability of GO is shifted to about 400 °C after incorporation with benzoxazine, which ascribed to

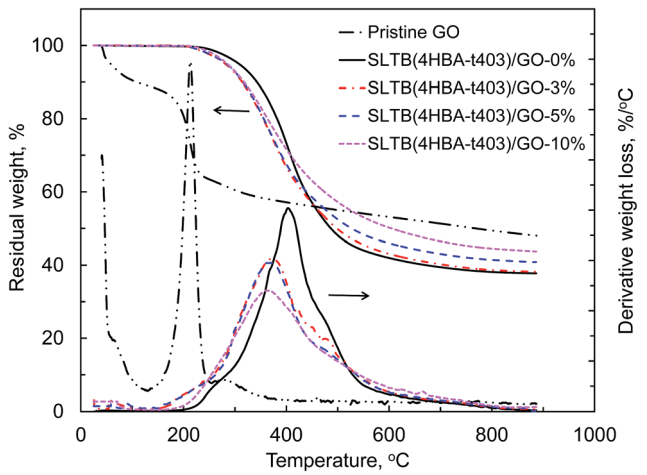

Fig. 12 TGA thermograms of aerogels obtained with different GO content.

Table 2 Summary of TGA data of the aerogels with different GO content

		Temperature of decomposition				
Sample code	T_{max} (°C)	T_{d5} (°C)	T_{d10} (°C)	T_{20} (°C)	T_{50} (°C)	Char yield (%)
Neat GO	211	57	109	201	797	49 ± 1
0 wt% GO	396	304	341	382	396	37 ± 2
3 wt% GO	364	280	314	355	498	39 ± 2
5 wt% GO	365	283	316	356	527	42 ± 3
10 wt% GO	367	285	318	363	605	45 ± 2

the strong interaction of benzoxazine structure with the functional groups of GO as early discussed.

As seen in Table 2, the maximum rate degradation temperature (T_{max}) of GO is 211 °C. However, the 5, 10, 20 and 50% weight loss temperatures (T_{d5}, T_{d10}, T_{d20}, and T_{d50}) of poly(SLTB(4HBA-t403)/GO) aerogels increased with GO-loading. For example, T_{d5} and T_{d10} for poly(SLTB(4HBA-t403)/GO-3%) are 280 and 314 °C, respectively, whereas T_{d5} and T_{d10} for poly(SLTB(4HBA-t403)/GO-10%) are 285 and 318 °C. The improved properties of polymerized nanocomposite aerogels may be due to the strong interactions with GO as discussed earlier. Additionally, the GO reinforced aerogels exhibited much lower degradation behavior at higher temperatures (>400 °C) than the neat polybenzoxazine aerogel, resulting in increased char yields, which is important property for preparing carbon aerogels. As seen in Table 2, the char yield at 800 °C of polybenzoxazine aerogel increased from 37 to 45% by loading 10 wt% GO. The char yield of GO is high since it is mostly carbon. Thus, increased the char yield of the obtained samples is expected. Therefore, polybenzoxazine/GO aerogels not only exhibit improved morphology than the neat polybenzoxazine aerogel, but also show excellent precursor for carbon aerogels. The char yield of benzoxazine aerogels increased significantly with GO content, primarily due to their strong interaction. To show the synergistic effect of GO-loading on the char yield of polybenzoxazine aerogels, the theoretical char yield for each nanocomposite aerogels was calculated. The theoretical char yield was obtained based on the composition of the sample and the actual char yield for neat both GO and polybenzoxazine, poly(SLTB(4HBA-t403)). The theoretical char yield value was calculated according to the eqn (3):

$$M_{total}\% = X_{PBZ}M_{PBZ}\% + (1 - X_{PBZ})M_{GO}\% \quad (3)$$

where: M_{total} is the theoretical value of char yield. M_{PBZ} is the char yield during TGA run of neat polybenzoxazine, PBZ. X_{PBZ} is the mass fraction of polybenzoxazine in the sample. M_{GO} is the char yield during TGA run of neat GO.

In order to investigate whether interactions existed between aldehyde-functional benzoxazine and GO, the theoretical and experimental values of char yield was compared. Fig. 13 displays the expected and experimental char yields of the nanocomposite aerogels. The char yields of the nanocomposites are higher than the theoretical prediction, which is attributed to

View Article Online
DOI: 10.1039/C5RA16188F
Paper

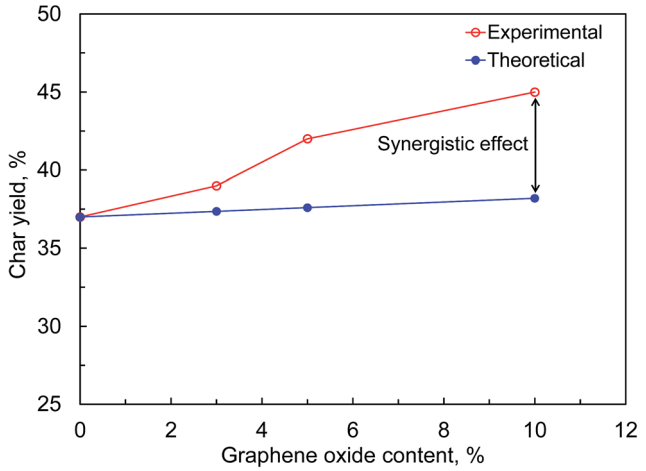

Fig. 13 Theoretical and measured char yield for polybenzoxazine aerogels with different GO content.

the synergism between polybenzoxazine and GO due to their strong interactions.

To summarize the TGA results, these nanocomposite aerogels derived from GO-reinforced polybenzoxazine exhibit more efficient for carbon aerogels than aerogels obtained from neat polybenzoxazine due to the increase in the char yield with increasing the GO content. Furthermore, the PBZ aerogels are mechanically stable due to the unique feature of PBZ for cross-linking ability.[7] In addition, presence of aldehyde groups enhances PBZ/GO interactions as investigated earlier. As a result of the network structure, the cross-linking contributes stiffness to the aerogels. These advantages make PBZ/GO hybrid aerogels as one of the strong candidates of aerogels for many applications.

4. Conclusions

Novel polybenzoxazine nanocomposites with three-dimensional (3D) porous materials have been successfully prepared by blending of star-like telechelic aldehyde-terminal-benzoxazine (SLTB(4HBA-t403)) with graphene oxide (GO) nanosheets. The 3D porous solids have been developed *via* freeze-drying of various colloidal dispersion of SLTB(4HBA-t403)/GO. Physicochemical interactions between aldehyde-terminal benzoxazine and GO interphases matrices led to hybridization. These interactions between functional groups of both SLTB(4HBA-t403) and GO are important in the formation of networks structure. FT-IR results indicated that during the heat treatment of SLTB(4HBA-t403)/GO aerogels, the aldehyde groups possibly oxidases and form carboxyl moieties. Therefore, ester formation results from chemical interaction SLTB(4HBA-t403) and GO *via* –OH and –COOH moieties. Furthermore, a strong hydrogen bonding is occurred between aldehyde-terminal benzoxazine and GO. The unique combination of intramolecular and intermolecular hydrogen bonding contributes to the properties of polybenzoxazine/GO aerogels. The XRD investigations indicated that GO is exfoliated in benzoxazine matrix up to 5 wt%, while slight residual GO aggregation was observed with 10 wt% GO. Morphological studies show that the aerogels exhibit porous nanostructure features. The presence of GO in polybenzoxazine aerogels plays a significant role in enhancing the morphological properties. The SEM images reveal that GO increases the layered structure of the aerogels and surface roughness. SEM micrographs of carbon aerogels show wrinkled and disordered GO-like sheets. The TEM results indicate good dispersion of GO in the polybenzoxazine matrix and pores have been observed in the nanometer scale. The DSC results indicated that addition of GO decreases the polymerization temperature of the SLTB(4HBA-t403). Compared to the neat polybenzoxazine aerogel, the nanocomposite aerogels show better thermal stability. The 50% weight loss temperature (T_{d50}) for aerogel and composite aerogels containing 3, 5, and 10 wt% GO are 498, 527, and 605 °C, respectively, while T_{d50} for neat polybenzoxazine aerogel is 396 °C. In addition, the char yield increased non-linearly with increasing GO content, showing synergism. Hybridization of benzoxazine aerogels with GO as highly porous structure of nanofiller provides special thermal and morphological properties of a new class of nanocomposite aerogels, which are expected to find various applications, such as in adsorption, catalytic, and conductive applications.

Acknowledgements

The Ministry of Education of Libya is acknowledged for the financial support in the form of a national scholarship to Almahdi Alhwaige. The authors thank Prof. Dr Schiraldi at Macromolecular Science and Engineering, Case Western Reserve University for his kind support.

References

1 S. S. Kistler, *J. Phys. Chem.*, 1932, **36**(1), 52–54.
2 C. Tan, B. M. Fung, J. K. Newman and C. Vu, *Adv. Mater.*, 2001, **13**, 644–646.
3 J. R. Johnson III, J. Spikowski and D. A. Schiraldi, *ACS Appl. Mater. Interfaces*, 2009, **1**, 1305–1309.
4 S. M. Alhassan, S. Qutubuddin and D. Schiraldi, *Langmuir*, 2010, **26**, 12198–12202.
5 A. I. Cooper and A. B. Holmes, *Adv. Mater.*, 1999, **11**, 1270–1274.
6 P. Lorjai, S. Wongkasemjit, T. Chaisuwan and A. M. Jamieson, *Polym. Degrad. Stab.*, 2011, **96**, 708–718.
7 H. Ishida, in *Handbook of Benzoxazine Resins*, ed. H. Ishida and T. Agag, Elsevier, Amsterdam, 2011, pp. 3–81.
8 T. Takeichi, R. Zeidam and T. Agag, *Polymer*, 2002, **43**, 45–53.
9 B. Kiskan, N. N. Ghosh and Y. Yagci, *Polym. Int.*, 2011, **60**, 167–177.
10 N. N. Ghosh, B. Kiskan and Y. Yagci, *Prog. Polym. Sci.*, 2007, **32**, 1344–1391.
11 Y. H. Wang, C. M. Chang and Y. L. Liu, *Polymer*, 2012, **53**, 106–112.
12 F. W. Holly and A. C. Cope, *J. Am. Chem. Soc.*, 1944, **66**, 1875–1879.
13 X. Ning and H. Ishida, *J. Polym. Sci., Part A: Polym. Chem.*, 1994, **32**, 1121–1129.
14 A. Chernykh, J. Liu and H. Ishida, *Polymer*, 2006, **47**, 7664–7669.

View Article Online
DOI: 10.1039/C5RA16188F
RSC Advances

15 P. Lorjai, T. Chaisuwan and S. Wongkasemjit, *J. Sol-Gel Sci. Technol.*, 2009, **52**, 56–64.
16 P. Katanyoota, T. Chaisuwan, A. Wongchaisuwat and S. Wongkasemjit, *Mater. Sci. Eng., B*, 2010, **167**, 36–42.
17 U. Thubsuang, H. Ishida, S. Wongkasemjit and T. Chaisuwan, *Microporous Mesoporous Mater.*, 2012, **156**, 7–15.
18 T. Chaisuwan, T. Komalwanich, S. Luangsukrerk and S. Wongkasemjit, *Desalination*, 2010, **256**, 108–114.
19 K. Pakkethati, A. Boonmalert, T. Chaisuwan and S. Wongkasemjit, *Desalination*, 2011, **267**, 73–81.
20 D. A. Rubenstein, H. Lu, S. S. Mahadik, N. Leventis and W. Yin, *J. Biomater. Sci., Polym. Ed.*, 2012, **23**, 1171–1184.
21 Q. C. Ran, Q. Tian, C. Li and Y. Gu, *Polym. Adv. Technol.*, 2010, **21**, 170–176.
22 N. Bitinis, M. Hernandez, R. Verdejo, J. M. Kenny and M. A. M. Lopez, *Adv. Mater.*, 2011, **23**, 5229–5236.
23 S. R. Hostler, A. R. Abramson, M. D. Gawryla, S. A. Bandi and D. A. Schiraldi, *Int. J. Heat Mass Transfer*, 2009, **52**, 665–669.
24 X. Fu and S. Qutubuddin, *Polymer*, 2001, **42**, 807–813.
25 P. Meneghetti and S. Qutubuddin, *Thermochim. Acta*, 2006, **442**, 74–77.
26 X. Chang, D. Chen and X. Jiao, *J. Phys. Chem. B*, 2008, **112**, 7721–7725.
27 M. Darder, P. Aranda and E. H. Ruiz, *Adv. Mater.*, 2007, **19**, 1309–1319.
28 K. K. Ho, M. C. Hsiao, T. Y. Chou, C. C. M. Ma, X. F. Xie, J. C. Chiang, S. H. Yang and L. H. Chang, *Polym. Int.*, 2013, **62**, 966–973.
29 M. Zeng, J. Wang, R. Li, J. Liu, W. Chen, Q. Xu and Y. Gu, *Polymer*, 2013, **54**, 3107–3116.
30 S. M. Alhassan, S. Qutubuddin, D. A. Schiraldi, T. Agag and H. Ishida, *Eur. Polym. J.*, 2013, **49**, 3825–3833.
31 J. Potts, D. R. Dreyer, C. W. Bielawski and R. S. Ruoff, *Polymer*, 2011, **52**, 5–25.
32 N. A. Kumar, H. J. Choi, Y. R. Shin, D. W. Chang, L. Dai and J. B. Baek, *ACS Nano*, 2012, **6**, 1715–1723.
33 J. Shen, Y. Hu, C. Li, C. Qin and M. Ye, *Small*, 2009, **5**, 82–85.
34 S. Stankovich, D. A. Dikin, R. D. Piner, K. A. Kohlhaas, K. Kleinhammes, Y. Jia, Y. Wu, S. B. T. Nguyen and R. S. Ruoff, *Carbon*, 2007, **45**, 1558–1568.
35 M. Seredych, A. V. Tamashausky and T. J. Bandosz, *Adv. Funct. Mater.*, 2010, **20**, 1670–1679.
36 D. A. Dikin, S. Stankovick, E. J. Zimney, R. D. Piner, G. H. B. Dommett, G. Evmenenko, S. T. Nguyen and R. S. Ruoff, *Nature*, 2007, **448**, 457–460.
37 F. Kim, J. L. Cote and J. Huang, *Adv. Mater.*, 2010, **22**, 1954–1958.
38 Y. Xue, Y. Liu, F. Lu, J. Qu, H. Chen and L. Dai, *J. Phys. Chem. Lett.*, 2012, **3**, 1607–1612.
39 A. Satti, P. Larpent and Y. Gun'ko, *Carbon*, 2010, **48**, 3376–3381.
40 X. Zhao, Q. Zhang and D. Chen, *Macromolecules*, 2010, **43**, 2357–2363.
41 M. A. Rafiee, J. Rafiee, Z. Wang, H. Song, Z. Z. Yu and N. Korathar, *ACS Nano*, 2009, **3**, 3884–3890.
42 J. Wang and M. W. Ellsworth, US Patent, 0144904, A1, 2010.
43 X. Zhang, Z. Sui, B. Xu, S. Yue, Y. Luo, W. Zhan and B. Liu, *J. Mater. Chem.*, 2011, **21**, 6494–6497.
44 A. A. Alhwaige, H. Ishida, T. Agag and S. Qutubuddin, *RSC Adv.*, 2013, **3**, 16011–16020.
45 N. Zhang, H. Qiu, Y. Si, W. Wang and J. Gao, *Carbon*, 2011, **49**, 827–837.
46 A. A. Alhwaige, Novel Biobased Chitosan/Polybenzoxazine Cross-Linked Polymers and Advanced Carbon Aerogels for CO_2 Adsorption, Ph.D. thesis, Case Western Reserve University, Cleveland, OH, USA, 2014.
47 F. Tuinstra and J. L. Koenig, *J. Chem. Phys.*, 1970, **53**, 1126.
48 T. C. Chieu, M. S. Dresselhaus and M. Endo, *Phys. Rev.*, 1982, **26**, 5867.
49 H. Ishida and D. Allen, *Polymer*, 1996, **37**, 4487–4495.
50 C. Jubsilp, K. Punson, T. Takeichi and S. Rimdusit, *Polym. Degrad. Stab.*, 2010, **95**, 918–924.
51 H. Ishida and Y. Roduriguez, *J. Appl. Polym. Sci.*, 1995, **58**, 1751–1760.
52 M. E. Smith and H. Ishida, *Macromolecules*, 1994, **27**, 2701–2707.
53 A. Tuzun, B. Kiskan, N. Alemdar, A. T. Erciyes and Y. Yagci, *J. Polym. Sci., Part A: Polym. Chem.*, 2010, **48**, 4279–4284.
54 C. Jubsilp, B. Ramsiri and S. Rimdusit, *Polym. Eng. Sci.*, 2012, **52**, 1640–1684.
55 J. Zhou, Z. Yao, Y. Chen, D. Wei, Y. Wu and T. Xu, *Polym. Compos.*, 2013, **34**, 1245–1249.
56 Q. C. Ran and Y. Gu, *J. Polym. Sci., Part A: Polym. Chem.*, 2011, **49**, 1671–1677.
57 A. A. Alhwaige, H. Ishida and S. Qutubuddin, Polybenzoxazine-based aerogels for CO_2 adsorption, unpublished work.
58 Y. C. Su, S. W. Kuo, D. R. Yei, H. Xu and F. C. Chang, *Polymer*, 2003, **44**, 2187–2191.
59 Y. C. Yen, C. C. Cheng, Y. L. Chu and F. C. Chang, *Polym. Chem.*, 2011, **2**, 1648–1653.
60 A. A. Alhwaige, T. Agag, H. Ishida and S. Qutubuddin, *Biomacromolecules*, 2013, **14**, 1806–1815.
61 B. Adhikari, A. Biswas and A. Banerjee, *ACS Appl. Mater. Interfaces*, 2012, **4**, 5472–5482.
62 V. C. Tung, J. Kim, L. J. Cote and J. Huang, *J. Am. Chem. Soc.*, 2011, **133**, 9262–9265.
63 Y. Zhao, H. Ding and Q. Zhong, *Appl. Surf. Sci.*, 2012, **258**, 4301–4307.
64 C. Pevida, T. C. Drage and C. E. Snape, *Carbon*, 2008, **46**, 1464–1474.
65 I. Zafiropoulou, M. S. Katsiotis, N. Boukos, M. A. Karakassides, S. Stephen, V. Tzitzios, M. Fardis, R. V. Vladea, S. M. Alhassan and G. Papavassiliou, *J. Phys. Chem. C*, 2013, **117**, 10135–10142.
66 L. Yang, C. Zhang, S. Pilla and S. Gong, *Composites, Part A*, 2008, **39**, 1653–1659.
67 J. Dunkers and H. Ishida, *J. Polym. Sci., Part A: Polym. Chem.*, 1999, **37**, 1913–1921.
68 H. C. Schniepp, J. L. Li, M. J. Mcallister, H. Sai, M. H. Alonso, D. H. Adamson, R. K. Prud'homme, R. Car, D. A. Saville and I. A. Aksay, *J. Phys. Chem. B*, 2006, **110**, 8535–8539.